Ballistic Thermal Conductance of a Lab-in-a-TEM Made Si Nanojunction

ARTICLE *in* NANO LETTERS · SEPTEMBER 2012

Impact Factor: 13.59 · DOI: 10.1021/nl302379f · Source: PubMed

6 AUTHORS, INCLUDING:

Laurent Jalabert
Laboratoire d'Analyse et d'Architecture des …

Tadashi Ishida
The University of Tokyo

Sebastian Volz
Ecole Centrale Paris

NANO LETTERS

Letter

pubs.acs.org/NanoLett

Ballistic Thermal Conductance of a Lab-in-a-TEM Made Si Nanojunction

L. Jalabert,[†] T. Sato,[‡] T. Ishida,[‡] H. Fujita,[‡] Y. Chalopin,[§,||] and S. Volz*,[†,§,||]

[†]LIMMS-CNRS/IIS-University of Tokyo, UMI CNRS 2820, 4-6-1 Komaba, Meguro-ku 153-8505 Tokyo, Japan

[‡]CIRMM-IIS University of Tokyo, 4-6-1, Komaba, Meguro-ku, 153-8505 Tokyo, Japan

[§]CNRS, UPR 288 Laboratoire d'Energétique Moléculaire et Macroscopique, Combustion, Grande Voie des Vignes, 92295 Chatenay-Malabry, France

[||]Ecole Centrale Paris, Grande Voie des Vignes, 92295, Châtenay-Malabry, France

Supporting Information

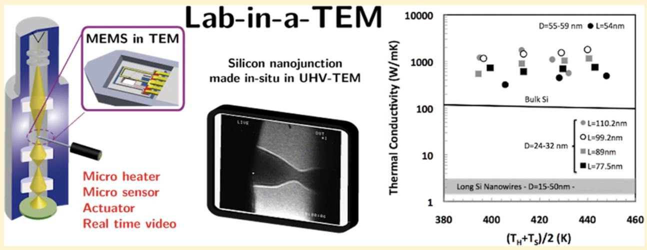

ABSTRACT: The thermal conductance of a single silicon nanojunction was measured based on a MEMS-in-TEM (microelectromechanical systems in a transmission electron microscope) technique and was found to be at least 2 orders of magnitude larger than the ones of long nanowires in the 380–460 K temperature range. The predominance of ballistic phonon transport appears as the best hypothesis to retrieve quantitative predictions despite the geometrical irregularity of the junction. The measurement is based on a MEMS structure including an electrostatic actuator that allows producing nanojunctions with the accuracy based on the resolution of a transmission electron microscope. The thermal conductance is measured by two integrated resistors that are simultaneously heating and measuring the local temperatures at the nearest of the nanojunction. The considerable thermal conductance of short nanojunctions constitutes a new key element in the design of nanosystems and in the understanding of the damaging of mechanical micronanocontacts. This conducting behavior is also paving the way for the development of nanoscale cooling devices as well as of the recent phononic information technology.

KEYWORDS: *MEMS, TEM, nanoscale heat transfer, ballistic, phonons, Lab-in-a-TEM*

Atomic to nanoscale solid-state device technologies have opened application fields involving new classes of physical phenomena. As such, phonon heat conduction is marked by the shift from a diffusive transport regime with predominant interactions between heat carriers to a ballistic one when the system size shrinks below the carrier mean free path.[1−9] In this latter case, the interaction with surfaces or interfaces governs the energy transport as shown for wires with micrometer scale diameters at a few kelvins[10] and nanowires with diameters of 15−20 nm at ambient temperature.[11−13] In one-dimensional structures where long wavelength phonons can exhibit direct ballistic flight from one end of the system to the other,[14−23] a very low quantified thermal conductance ($3.77 \times 10^{-12} \times T$ W/K) can be observed in specific acoustically adapted junctions at temperatures lower than 2 K.

In this Letter, we show that the existence of ballistic thermal phonons has to be assumed at temperatures ranging between 380 K and 460 K to explain our experimental data. This behavior is revealed by measuring the thermal conductance of a suspended nanojunction formed by atomic rearrangement of silicon atoms between two silicon tips, then elongated to vary its length between 54 nm and 110 nm. High thermal conductance values that are several orders of magnitude larger than those expected from the experimental data obtained in long nanowires tend to confirm ballistic transport inside the wire. Those observations open a new field of properties and of physical mechanisms in nanostructures with unequaled small sizes.

Even still far from what the nature itself can make,[24] several atomic-scale engineering methods have emerged from the manipulation of individual atom assisted by scanning tunnelling microscope (STM) tips,[25] with long-term perspectives in developing single molecule information devices. A need for real-time observation and control of such atomic manipulations has motivated significant progress in transmission electron microscopy (TEM) hardware, especially with the in situ mounting of STM tips.[26] In the 1990s, TEM holders were significantly improved with adding piezoelectric actuator leading to impressive atomic chains formation and elongation between two tip apexes, as revealed by real-time TEM videos. Such atomic manipulation paved the way for in situ electrical, mechanical, and structural characterizations of metallic,[27−31] semiconductor,[33] or magnetic nanojunctions.[34] Continuous

Received: June 26, 2012
Revised: September 16, 2012

efforts in implementing TEM holder with heaters[35] or gas injectors[36] have yielded the emergence of a "Lab-in-a-TEM".

However, no report has been dedicated so far to the study of nanoscale heat transfer through suspended atomic chains made in situ in TEM. The main reason is that the integration of local heater, local temperature sensor, and accurate actuator has remained a hurdle due to the lack of space on TEM holder. Such space limitations can be easily overcome by using microelectromechanical systems (MEMS) that offer a higher integration level.[37] Nanoscale friction using 2D electrostatic actuators[38] or the observation of in-liquid dynamic phenomena[39,40] illustrates the promising of "Lab-in-a-TEM" using MEMS.

Experimental Setup and Protocol. To produce nanojunctions, we have here designed and fabricated a MEMS device including an electrostatic actuator that controls the subnanometer displacements of a movable tip facing a fixed one as illustrated in Figure 1 (Supporting Information, Movie 1).

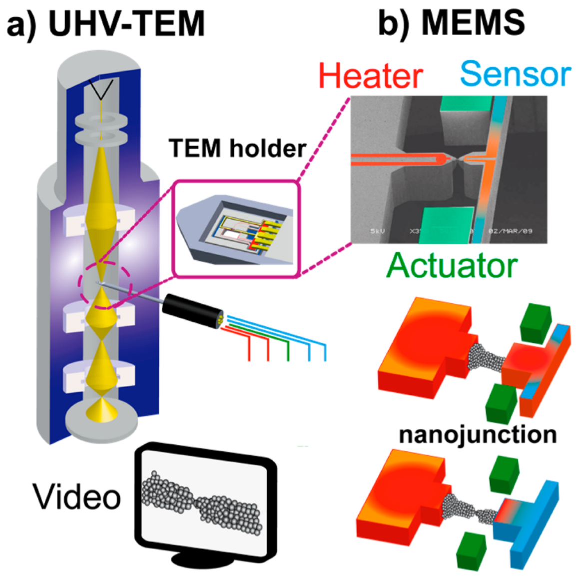

Figure 1. (a) Schematic view of the UHV-TEM with real-time video recording. The MEMS device is mounted on a special holder with electrical feedthroughs connected to instruments. (b) SEM view of the MEMS device with unrealistic colors showing the integrated microheater (red) on a fixed tip, temperature sensor (blue) on the movable tip, and an electrostatic actuator (green). A silicon nanojunction is formed between the opposing tips and elongated by pulling the movable tip in TEM (see Supporting Information, Movie 1).

After bringing tips into contact gently, we produce a single nanojunction by moving the tip backward from the contact position. This junction formation is attributed to a local rearrangement of silicon atoms.[37] TEM observation is then required to track and control the silicon nanojunction formed between the opposing tips. The electrostatic actuator has superior stability compared to the one of a conventional piezoactuator and a precise control over long period of time (more than ~8 h experiments).

Figure 1 also shows that the MEMS is composed of integrated microresistors on both tips; one of those is used as a thermometer and a heater, whereas the other one serves as a temperature sensor only. Local Joule heating is generated by applying a bias current on the heater resistance, which yields an increase δT_h of the temperature at the tip with respect to the bath temperature T_a of the TEM environment. A fraction of the produced heat will be transferred through the nanojunction and will raise the tip temperature on the sensor side by δT_s. The integration of metallic resistances on suspended microstructures may induce bending artifacts during Joule heating cycles due to the mismatch between thermal expansion coefficients. To avoid this issue, the microresistances are made of heavily boron-doped silicon deposited by LPCVD. The boron concentration in the 250-nm-thick layer is near the limit of solubility of boron in silicon ($\sim 10^{21}$ at/cm^3) and uniformly distributed in the volume after annealing, which is usually a difficult task to achieve. Consequently, nanoscale bending or other thermally induced artifacts were not observed during the Joule heating experiments. The initial heater and sensor resistances measured in vacuum condition are 6 kΩ and 16 kΩ, respectively. The heater and sensor elements are electrically insulated by a 2-μm-thick oxide from the SOI wafer. Leakage current as low as a few 50 pA was measured between the heater and sensor pads, which remains within the noise level of the instrument.

The calibration of the temperature dependent resistance is performed in a vacuum probe station (Janis RT-500-1) at a nominal pressure of 350 Pa to avoid convection effects. The temperature dependence of the current–voltage characteristics confirms an ohmic behavior (see Supporting Information, Movie 2) of the planar microresistances. The calibration is performed in the same electrical conditions as TEM experiments and allows converting the variations of the sensor resistance into the corresponding variation of temperature for each heating and cooling sequence.

In ultrahigh vacuum conditions (5×10^{-8} Pa), silicon nanowires were formed between the heater and the sensor areas by simply retracting one tip slowly (after gently bringing them into contact) to generate a nanowire of a maximum length of 110 nm between the two silicon tips. Figure 2a shows

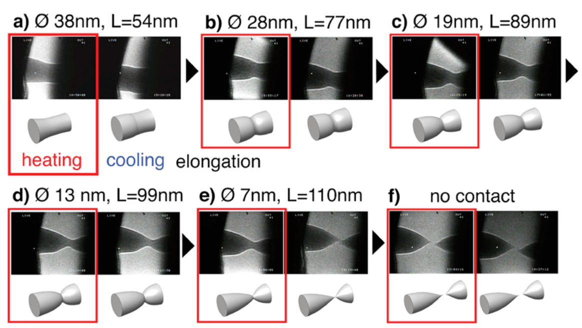

Figure 2. TEM images of the nanowire. Image a represents the junction with a 54 nm length. Images b, c, d, and e report the wire geometry when pulling it up to lengths of 77.5 nm, 89 nm, 99.2 nm, and 110.2 nm, respectively (see Supporting Information, Movie 3). The reported diameters are those of the constrictions.

a junction 54 nm in length, which was then pulled, and the thermal conductances of wires having lengths of 77.5 nm, 89 nm, 99.2 nm, and 110.2 nm were measured. Figure 2b–e shows a constriction in the midregion of those wires (see Supporting Information, Movie 3) whereas the 2a junction appears as cylindrical in the latter phase of the measurement.

For a given nanojunction, heating/cooling cycles were provided by applying a heater current with values of 0.3, 0.5, 0.8, 1.2, 1.8, and 2 mA during the first hundred seconds and by turning off the current during the following hundred seconds. During each cycle, the heater voltage was measured, and the sensor current was obtained at a constant voltage bias of −0.5 V (see Supporting Information, Movie 4). Sensor and heater electrical resistances could then be deduced and yielded the average temperature increase in the resistance volumes from the calibration curve. For the L = 54 nm junction and a total injected power of 15 mW, the heater averaged temperature increased by 70 K, while the sensor average temperature rise was estimated to 18 K. The relevance of our measurement was clearly proven at the end of the experiment because the temperature rise calculated from the sensor signal returned to zero at the same time as the silicon wire was broken.

To deduce the local temperature in the vicinity of the junction, a finite element modeling of the heater and the sensor was carried out. A homogeneous Joule power was defined inside the heater resistance volume, and the corresponding tip and resistance temperatures were calculated. The ratio between those two latter temperatures was found independent of the input Joule power and considered as a relevant correction factor (Supporting Information, Movie 5).

The thermal conductance G_J of the nanojunction was finally determined from δT_H and δT_S by stating the heat flux conservation through the junction and the sensor supporting beam characterized by the conductance G_S:

$$G_J^{ex} = G_S \frac{\delta T_S}{\delta T_H - \delta T_S} \qquad (1)$$

G_S was then derived from a finite element modeling of the sensor tip and its supporting beam by applying a heat flux on the junction area and by computing the temperature difference between the tip and the beam ends. The ratio between flux and temperature directly yields G_S = 308 μW/K (see Supporting Information, Movie 5). The uncertainty error on the device dimensions due to the fabrication technique added to the one on the silicon thermal conductivity yields an overall figure of 11%. Note that the measured temperature difference appearing in the denominator of eq 1 was found to be significantly larger than the sensor temperature variation δT_S, which ensures a robust estimation of the temperature ratio. The experimental data will however reveal that the stability of the nanojunction structure is the main source of inaccuracy because it can range from a few percent to more than 50%.

Physical Model. Predominant heat carriers in doped silicon are phonons, that is, quanta of the lattice elastic energy. The predominant phonon wavelength at temperatures between 380 K and 460 K can be estimated to a few nanometers and remains lower than the junction diameter. Confinement is therefore not expected, and a three-dimensional phonon transport is considered. As proposed in previous articles, the prevalence of surface scattering in the 300−500 K temperature range in long nanowires reduces the phonon mean free path and yields a low effective thermal conductivity of 1.5−3 W·m^{-1}·K^{-1} for diameters ranging from 15 to 30 nm.[12] In our experiments involving very short wires, the number of scattering events with the surface is considerably reduced. We therefore a priori consider that this mechanism can be considered as negligible a priori and ballistic phonon transport should then be assumed as predominant. To confirm this assumption, we express the ballistic conductance between the junction ends by using Sharvin's Law:[19]

$$G_J^{th} = \pi C_p v S_J \qquad (2)$$

where v is the mean Si phonon group velocity and C_p is the Si heat capacity. From previous analysis[41] within the framework of the Debye model, v = 6400 m·s^{-1} and C_p = 1.66 × 10^6 J·K^{-1}·m^{-3}. S_J refers to the nanojunction cross section. A former work[42] has confirmed that this latter cross section is cylindrical by studying the mechanical properties of the junction. We have also confirmed this fact by analyzing the contrast information on the basis of the Beer's Law of absorption.

Results and Discussion. In Figure 3a, the nanowire thermal conductance obtained from experimental data and eq 1

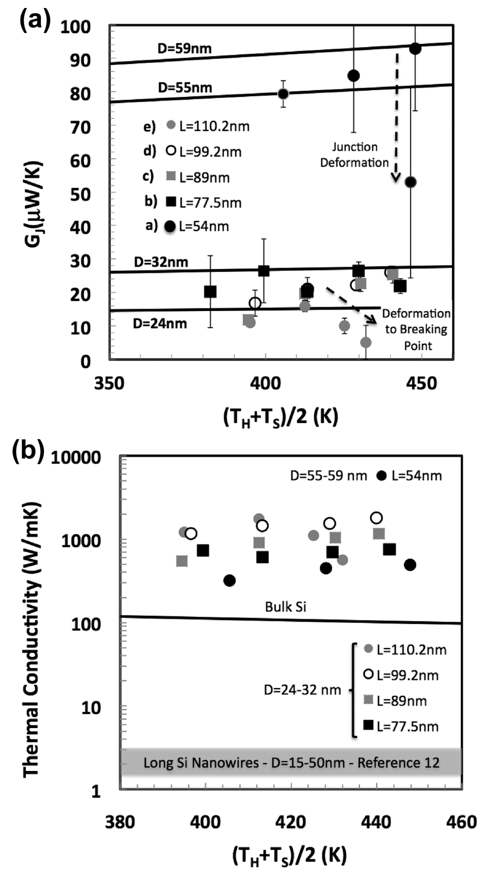

Figure 3. (a) Thermal conductances of the wires reported in Figure 2a to e versus temperatures. Data points refer to experimental data and lines to theoretical predictions of eq 2. (b) Effective thermal conductivity of Si nanojunctions (data points) and long Si nanowires (gray zone as indicated in ref 3) and bulk thermal conductivity (continuous line) as a function of temperature.

was reported as a function of the mean temperature $(T_H + T_S)/2$ in the geometrical configurations defined in Figure 2. The black disks refer to Figure 2a where the junction is 54 nm in length. The black and gray squares correspond to Figure 2b and c, respectively; the black circles and the gray disks also represent the results obtained in the situations of Figure 2d and e, respectively. The black lines are derived from the theoretical predictions of eq 2 when the wire diameter equals to D = 59, 55, 32, and 24 nm.

For the structures of Figures 2b−e resembling to two half ellipsoids in contact, the experimental data strikingly remain in a narrow range of conductance values defined by the theoretical trends for D = 32 nm and D = 24 nm. This diameter can be

dx.doi.org/10.1021/nl302379f | Nano Lett. XXXX, XXX, XXX−XXX

reasonably compared to the diameter of the smallest wire/substrate contact area, which is the right side contact in Figure 2b−e. In other words, the junction thermal conductance does not seem to be sensitive to the wire shape between the two contacts but only to its wire/substrate contact with smallest cross section. This can be considered as a confirmation of the absence of surface scattering inside the wire and the ballistic nature of phonon transport. Note that the 7 nm constriction case has yielded large error bars at high input powers due to the structural deformation and breakdown.

The L = 54 nm diameter case under highest heater temperatures revealed a structural change as revealed by the junction shapes in the first and the last phase of the measurement reported in Figure 2a. The thermal conductance was found to be highly sensitive to this change, which yielded 20% and then 50% error bars. The junction diameter after cooling was found to be 52 nm in Figure 2a, whereas theoretical predictions with D = 55 nm and D = 59 nm could frame the mean values. As highlighted by the error bars, we believe that surface diffusion at high temperatures have produced diameter fluctuations that might explain this 6−12% diameter difference.

The reasonable agreement between theoretical and experimental data confirms that phonons are indeed crossing the short nanowire without any scattering events, neither through phonon−phonon collisions nor through phonon−surface interactions. The consequence of this specific phenomenon is the apparition of a thermal conductance 2 orders of magnitude higher than the one reported in the literature.[12]

This trend is somehow unexpected because: (i) the junction structure is rather uncertain and might be amorphous; in this situation, internal scattering should be predominant at least for higher frequency phonons with reduced phonon mean free path of a few angstroms and (ii) until now, the absence of surface scattering was only observed at extremely low temperatures below 2 K in long nanowires where only one-dimensional or axial propagation is involved. To sum up, the nanowire acts here as a perfect thermal conductor as if the two heat baths were in direct contact. The junction thermal resistance is only generated by the limited phonon specific heat and velocities in those heat baths.

In Figure 3b, the nanojunction effective thermal conductivities are compared with the thermal conductivities of the bulk silicon (solid line) and the long nanowires (gray zone) from ref 12. Those thermal conductivity values are purposely called "effective" because they do not correspond to a diffusive regime of phonon transport. They however highlight the efficiency of the heat transfer in the junction. They were estimated by considering the fictive validity of the heat conduction equation in the nanojunctions, which are either cylindrical (Figure 2, case a) or biconical (Figure 2, cases b−f). In this latter case, the thermal conductivity is derived from a two-cones model: G $(L_1/S_1 + L_2/S_2)$ where $L_{1,2}$ and $S_{1,2}$ are the lengths and apparent cross sections of cones 1 and 2. Those latter cross sections are derived without approximation from the maximum and minimum cone cross sections S_{max} and S_{min} as $(S_{max} - S_{min})/\ln(S_{max}/S_{min})$. The long nanowire thermal conductivity finally appears to be 2−3 orders of magnitude smaller than the ones of nanojunctions. We note a consistent progression of the effective thermal conductivity with the nanojunction length.

Conclusion. We have measured the thermal resistance of a single irregular silicon nanojunction by using a MEMS that drives facing tips with subnanometer resolution. This device also integrates a microheater on one tip and a thermoresistive microsensor on the other, both designed very closed to the nanojunction. The whole microsystem is inserted in a TEM to control the gap between two tips and to observe the formation of nanowires. The obtained effective thermal conductivity appears to be at least 2 orders of magnitude larger than the ones obtained for long nanowires. A purely ballistic description of phonon transport without boundary scattering yields a satisfying prediction of the experimental data. This agreement tends to confirm the presence of ballistic phonons between 380 K and 460 K, whereas this behavior is usually observed at low temperatures in wires with acoustically adapted contacts. This outcome is opening new possibilities in the design of nanodevice cooling as well as of phonon information and communication technologies.[43]

■ ASSOCIATED CONTENT

Ⓢ Supporting Information

Movie M1: elongation from 54 nm to 77 nm (si_m1.avi). Movie M2: elongation from 77 nm to 89 nm (si_m2.avi). Movie M3: elongation from 89 nm to 99 nm (si_m3.avi). Movie M4: elongation from 99 nm to 110 nm (si_m4.avi). This material is available free of charge via the Internet at http://pubs.acs.org.

■ AUTHOR INFORMATION

Corresponding Author

*E-mail: sebastian.volz@ecp.fr; volz@em2c.ecp.fr.

Notes

The authors declare no competing financial interest.

■ ACKNOWLEDGMENTS

We gratefully acknowledge Prof. R. F. Egerton from University of Alberta (Canada) for valuable discussions relative to electron beam heating in TEM, Mr. Yoshihumi Ueda from Hitachi Japan for technical discussion relative the UHV-TEM HF-2000, and M.-C. Tahran (University of Tokyo) for fruitful discussions related to thickness analysis. We acknowledge also CNRS-LAAS (Toulouse), especially Mr. F. Carcenac for his expertise on TEM, Dr. E. Scheid, B. Rousset, and L. Bouscayrol for the heavily boron doped silicon layer deposited on our substrate using a prototype of vertical LPCVD furnace. We gratefully thank Mr. Rolf Vermeer from University of Twente (The Netherlands) for developing image processing toolboxes that was adapted by the authors for evaluating the elongation of the junctions from the video analysis. This work was supported by KAKENHI; the grant-in-aid of Scientific (S) 16191004 and Specially Promoted Research 21000008 sponsored by the Japan Society for the Promotion of Science (JSPS).

■ REFERENCES

(1) Hochbaum, A. I.; Chen, R.; Delgado, R. D.; Liang, W.; Garnett, E. C.; Najarian, M.; Majumdar, A.; Yang, P. Enhanced thermoelectric performance of rough silicon nanowires. *Nature* **2008**, *451*, 163−167.

(2) Vo, T. T. M.; Williamson, A. J.; Lordi, V.; Galli, G. Atomistic Design of Thermoelectric Properties of Silicon Nanowires. *Nano Lett.* **2008**, *8*, 1111.

(3) Volz, S.; Chen, G. Molecular Dynamics Simulation of Thermal Conductivity of Silicon Nanowires. *Appl. Phys. Lett.* **1999**, *57*, 2056.

(4) Volz, S.; Lemonnier, D. Confined Phonon and Size Effects on Nanowire Thermal Conductivity. The Radiative Transfer Approach. *Phys. Low-Dimen. Struct.* **2000**, *5/6*, 91.

(5) Zou, J.; Balandin, A. Phonon heat conduction in a semiconductor nanowire. *J. Appl. Phys.* **2001**, *89*, 2932.

(6) Khitun, A.; Wang, K. L. Modification of the three-phonon Umklapp process in a quantum wire. *Appl. Phys. Lett.* **2001**, *79*, 851.
(7) Mingo, N. Calculation of Si nanowire thermal conductivity using complete phonon dispersion relations. *Phys. Rev. B* **2003**, *68*, 113308.
(8) Chantrenne, P.; Barrat, J. L.; Blase, X.; Gale, J. D. An analytical model for the thermal conductivity of silicon nanostructures. *J. Appl. Phys.* **2005**, *97*, 104318.
(9) Lacroix, D.; Joulain, K.; Terris, D.; Lemonnier, D. Monte Carlo simulation of phonon confinement in silicon nanostructures: Application to the determination of the thermal conductivity of silicon nanowires. *Appl. Phys. Lett.* **2006**, *89*, 103104.
(10) Heron, J. S.; Fournier, T.; Mingo, N.; Bourgeois, O. Mesoscopic Size Effects on the Thermal Conductance of Silicon Nanowire. *Nano Lett.* **2010**, *10*, 2288.
(11) Li, D.; et al. Thermal conductivity of individual silicon nanowires. *Appl. Phys. Lett.* **2003**, *83*, 2934−2936.
(12) Chen, R.; Hochbaum, A. I.; Murphy, P.; Moore, J.; Yang, P.; Majumdar, A. Thermal Conductance of Thin Silicon Nanowires. *Phys. Rev. Lett.* **2008**, *101*, 105501.
(13) Donadio, D.; Galli, G. Atomistic Simulations of Heat Transport in Silicon Nanowires. *Phys. Rev. Lett.* **2009**, *102*, 195901.
(14) Greiner, A.; Reggiani, L. Thermal Conductivity and Lorenz Number for One-Dimensional Ballistic Transport. *Phys. Rev. Lett.* **1997**, *78*, 1114.
(15) Greiner, A., L.; Kuhn, T. Comment on "Quantized Thermal Conductance of Dielectric Quantum Wires". *Phys. Rev. Lett.* **1997**, *81*, 5037.
(16) Rego, L. G. C.; Kirczenow, G. Quantized Thermal Conductance of Dielectric Quantum Wires. *Phys. Rev. Lett.* **1998**, *81*, 232.
(17) Cross, M. C.; Lifshitz, R. Elastic wave transmission at an abrupt junction in a thin plate with application to heat transport and vibrations in mesoscopic systems. *Phys. Rev. B* **2001**, *64*, 85324.
(18) Chang, C. M.; Geller, M. R. Mesoscopic phonon transmission through a nanowire-bulk contact. *Phys. Rev. B* **2005**, *71*, 125304.
(19) Prasher, R. Predicting the Thermal Resistance of Nanosized Constrictions. *Nano Lett.* **2005**, *5*, 2155.
(20) Chalopin, Y.; Gillet, J.-N.; Volz, S. Predominance of Thermal Contact Resistance in Connected Silicon Nanowires. *Phys. Rev. B* **2008**, *77*, 233309.
(21) Venkatesh, R.; Amrit, J.; Chalopin, Y.; Volz, S. Thermal resistance of metal nanowire junctions in the ballistic regime. *Phys. Rev. B* **2011**, *83*, 115425.
(22) Schwab, K.; Henriksen, E. A.; Worlock, J. M.; Roukes, M. L. Measurement of the Quantum of Thermal Conductance. *Nature* **2000**, *404*, 974−977.
(23) Chiatti, O.; Nicholls, J. T.; Proskuryakov, Y. Y.; Lumpkin, N.; Farrer, I.; Ritchie, D. A. Quantum Thermal Conductance of Electrons in a One-Dimensional Wire. *Phys. Rev. Lett.* **2006**, *97*, 56601.
(24) Wang, J. Can man-made nanomachines compete with nature biomotors? *ACS Nano* **2009**, *3*, 4−9.
(25) Becker, R. S.; et al. Atomic-scale surface modifications using a tunnelling microscope. *Science* **1987**, *325*, 419−421.
(26) Iwatsuki, M.; et al. Scanning-tunnelling microscope (STM) for conventional transmission electron microscope (TEM). *J. Electron. Microsc.* **1991**, *40*, 48−53.
(27) Kondo, Y; Takayanagi, K. Gold nanobridge stabilized by surface structure. *Phys. Rev. Lett.* **1997**, *79*, 3455−3458.
(28) Kizuka, T.; et al. Cross-sectional time-resolved high-resolution transmission electron microscopy of atomic-scale contact and noncontact-type scannings on gold surfaces. *Phys. Rev. B* **1997**, *55*, 7398−7401.
(29) Kondo, Y.; Ohnishi, H. Quantized conductance through individual rows of suspended gold atoms. *Nature* **1998**, *395*, 780−783.
(30) Kizuka, T. Atomic process of point contact in gold studied by time-resolved high-resolution transmission electron microscopy. *Phys. Rev. Lett.* **1998**, *81*, 4448−4451.
(31) Rodrigues, V.; et al. Signature of atomic structure in the quantum conductance of gold nanowires. *Phys. Rev. Lett.* **2000**, *85*, 4124−4127.
(32) Bettini, J.; et al. Experimental realization of suspended atomic chains composed of different atomic species. *Nat. Nanotechnol.* **2006**, *1*, 182−185.
(33) Kizuka, T.; et al. Measurements of the atomistic mechanics of single crystalline silicon wires of nanometer width. *Phys. Rev. B* **2005**, *72*, 035333.
(34) Rodrigues, V.; et al. Evidence for Spontaneous Spin-Polarized Transport in Magnetic Nanowires. *Phys. Rev. Lett.* **2003**, *90*, 096801.
(35) Naitoh, Y.; et al. Simultaneous STM and UHV electron microscope observation of silicon nanowires extracted from Si (111) surface. *J. Elect. Microsc.* **2000**, *49*, 211−216.
(36) Saka, H.; et al. "In Situ" Heating Transmission Electron Microscopy. *MRS Bull.* **2008**, *33*, 93−100.
(37) Ishida, T.; et al. Design and fabrication of MEMS-controlled probes for studying the nano-interface under in situ TEM observation. *J. Micromech. Microeng.* **2010**, *20*, 075011.
(38) Sato, T.; et al. Development of MEMS-in-TEM Setup to Observe Shear Deformation for the Study of Nano-Scale Friction. *Tribol. Online* **2011**, *6*, 226−229.
(39) Grogan, J. M.; Bau, H.-H. The nanoaquarium: a platform for in-situ transmission electron microscopy in liquid media. *J. Microelectromech. Syst.* **2010**, *19*, 885−894.
(40) de Jonge, N.; Ross, F. M. Electron microscopy of specimen in liquid. *Nat. Nanotechnol.* **2011**, *6*, 695.
(41) Chen, G. Thermal conductivity and ballistic-phonon transport in the cross-plane direction of superlattices. *Phys. Rev. B* **1998**, *57*, 14858.
(42) Ishida, T.; Cleri, T.; Kakushima, K.; Mita, M.; Sato, T.; Miyata, M.; Itamura, N.; Endo, J.; Toshiyoshi, H.; Sasaki, N.; Collard, D.; Fujita, H. Exceptional plasticity of silicon nanobridges. *Nanotechnology* **2011**, *22*, 355704.
(43) Li, N.; Ren, J.; Wang, L.; Zhang, G.; Hänggi, P.; Li, B. Colloquium: Phononics: Manipulating heat flow with electronic analogs and beyond. *Rev. Mod. Phys.* **2012**, *84*, 1045.